65^{th} International Astronautical Congress 2014, Toronto, Canada.

IAC-14-C1.6.13

A FEASIBILITY STUDY OF SOLAR RADIATION PRESSURE FEEDBACK CONTROL STRATEGY FOR UNSTABLE PERIODIC ORBITS IN THE RESTRICTED THREE-BODY PROBLEM

Stefania Soldini
Astronautics Research Group, University of Southampton, Southampton, United Kingdom, s.soldini@soton.ac.uk

Camilla Colombo
Department of Aerospace Science and Technology, Politecnico di Milano, Milano, Italy, camilla.colombo@polimi.it

Scott Walker
Astronautics Research Group, University of Southampton, Southampton, United Kingdom, sjiw@soton.ac.uk

This paper investigates a Hamiltonian structure preserving control strategy that uses, where possible, solar radiation pressure as an alternative propellant-free control acceleration. This control strategy is based on previous authors work, but it is extended to a general case in which complex and conjugate eigenvalues occur at high amplitude orbits. High amplitude orbits are currently of interest to the European Space Agency (ESA) for future Libration-points orbits space missions since a lower insertion ΔV is required to reach these orbits by saving propellant. This control aims to stabilise the LPOs in the sense of Lyapunov by achieving simple stability, and it preserves the Hamiltonian nature of the controlled system. Based on the design of the feedback control, the purpose of this work is to verify when the use of SRP is feasible. Indeed, the order of magnitude of solar radiation pressure acceleration depends on the spacecraft's reflective area, the area orientation angle and its reflectivity properties. Therefore, due to constraints in the orientation angle and in the deployable reflective area, it is important to identify when, along the spacecraft's trajectory it is possible to apply SRP to stabilise the unstable periodic orbit. This limitation in the actuator causes the "windup" of the controller; thus, the use of desaturation methods are investigated.

I INTRODUCTION

Missions to study the Sun or planetary satellites, or to observe the Universe require the selection of a convenient operational orbit to guarantee constant geometry during observations, a good communication relay between the spacecraft and the Earth and to fulfil the constrains of thermal design. In 1968, Farquhar proposed to exploit periodic orbits around the Lagrangian-points of the Earth-Moon system also known as Libration-Point Orbits (LPOs). Orbits around L_1 and L_2 are relatively inexpensive to be reached via a direct launch from Earth and they ensure the previously mentioned mission requirements (1). LPOs are also selected since they are gateway orbits (i.e., heteroclinic connections) within the Sun-Earth system. The interest of the space agencies in LPOs started after the success of ISEE-3 mission in 1978. Current example of LPO missions include SOHO that studies the Sun's outer corona (2), and Herschel to investigate the formation of galaxies (3). The European Space Agency (ESA) just succeeded in launching the Gaia space telescope (4), while NASA/ESA/CSA's James Webb Space Telescope will provide astronomical measurements to understand the formation of our Universe and ESA's Euclid will map the geometry of the dark Universe (5). Distant Prograde Orbits (DPOs) are instead periodic orbits around the smaller

body; also known as second primary (6) (i.e., the Earth in the Sun-Earth system). Lara et al. (7) suggested the use of DPOs for studying the planetary satellites of a general system, for example to study the asteroid in the Sun-Asteroids system (8), or planets in the Sun-Planet system.

However, LPOs and DPOs lie in highly chaotic regions; therefore, an uncontrolled spacecraft would naturally follow the stable and unstable manifolds. Thus, the instabilities let trajectories transfer within the L_1 and L_2 families of periodic orbits as demonstrated by the NASA's Wind spacecraft (9).

When looking at the Sun-Earth system, one of the major perturbations after the gravitational effects is the Solar Radiation Pressure (SRP). Environmental perturbations cause instabilities to LPOs, where monthly station-keeping manoeuvres are constantly required to counteract their effects (10). An alternative idea is to design control strategies based on the exploitation of orbit perturbations, to allow a significant reduction in the amount of required on-board propellant. The SRP acceleration magnitude is a function of the spacecraft's area-to-mass ratio, the control area orientation angle and the material reflectivity properties. Thus, reflective deployable structures can potentially control the spacecraft through SRP acceleration to perform station-keeping. Indeed, the first concept of SRP stabilisation was proposed for attitude control in 1959 (11), and geosynchronous satellites such as OTS, TELECOM 1 and INMARSAT 2 have successfully implemented control strategies based on SRP. An asymmetrical offset of solar array wings from the nominal sun-pointing orientation is maintained to generate "wind-mill" torques and additional solar flaps mounted on the solar array can enhance their effects.

The aim of this research is to develop a feedback control strategy that can be performed by a propellant-free system, which uses SRP, where possible, to stabilise the spacecraft's trajectory. Different concept solutions by using existing on-board deployable structures to enhance SRP will be investigate. A Hamiltonian Structure Preserving (HSP) control strategy was selected and previously compared with the Floquét Mode (FM) control since these strategies exploit the natural dynamics of the system (12). HSP showed its robustness due to failure in the halo orbit injection manoeuvres, while FM can not stabilise unstable LPOs when the controller is pushed to work in a highly non-linear regime. Thus, HSP showed to be a good candidate for SRP applications since it is robust, it works in non-linearities conditions and the overall required ΔV is low in comparison to FM requirements.

The HSP control proposed in this work is based on the work of Scheeres et al. (13) and M. Xu and S. Xu (14), but it is extended to a general case, in which complex and conjugate eigenvalues (i.e., stable-unstable focii) occur. Indeed, the HSP designed by previous authors can control a trajectory in the case the planar equilibrium is hyperbolic×center. Our interest is to apply the control to high amplitude orbits, as they allow reducing the overall ΔV required for transfer and maintenance (15). The HSP controller is designed to ensure simple Lyapunov stability by exploiting the stable and unstable manifolds directions, by creating an artificial center manifold. The extended HSP control law was successfully tested for SOHO mission and for high amplitude DPOs and planar-Lyapunov (12). Both the test cases shows that the HSP controller that is limited to treat hyperbolic×center equilibrium fails at high amplitudes, due to the local occurrence of couples of complex and conjugate eigenvalues of the linearised system.

In this paper, the proposed HSP algorithm for high amplitude orbits is derived. Particular focus is given to the selection of gain set. Then, the HSP control is applied to the use of SRP; where, the actuator's model add constrains to the system. It is well-known that the constrains in the actuators can have an important impact on the behaviour of the feedback control system, by causing the degradation of the control performances. This occurs when a saturation non-linearity is added to the feedback control. This phenomena is known as "windup" where the saturation non-linearity slows down the response of the feedback and thus causes the integrator state to "windup" to excessively large values (16).

There are several possibilities to avoid saturation: one is to implement anti-windup schemes (16) as for example nested saturations (17), direct linear anti-wind up or model recovery anti-windup. However, if the control actuators are continuously trying to act beyond their limits, it should be investigated the redesign of the control law to include the effect of saturation directly in the control design.

This paper is organised as follows: Section II focuses on the equations of motion, while in Section III the HSP control law to extended high amplitude orbits is derived. Then, the condition for the gains selection is demonstrated in Section IV and the shape of the artificial potential energy is shown in Section V. Section VI shows the controllability of the unconstrained close-loop control and Section VII describes how to model the actuator subsystem. Finally, Section VIII investigates the effect of the actuator saturation on the system.

II DYNAMICAL MODEL

The spacecraft's dynamics is described by the Circular Restricted-Three Body Problem under the influence of Solar Radiation Pressure, (CRTBPS). The equations of motion are written with respect to a rotating frame in dimensionless coordinates;

$$\begin{cases} \ddot{x} - 2\omega_0\dot{y} = \bar{V}_x(x,y,z) + a_x^s(x,y,\beta,\alpha,\delta) \\ \ddot{y} + 2\omega_0\dot{x} = \bar{V}_y(x,y,z) + a_y^s(x,y,\beta,\alpha,\delta) \\ \ddot{z} = \bar{V}_z(x,y,z) + a_z^s(x,y,\beta) \end{cases} \quad [1]$$

where, x, y, z and $\dot{x}$, $\dot{y}$, $\dot{z}$ are the spacecraft positions and velocities in the rotating frame. The spacecraft's mass is assumed to be infinitesimal with respect to the Sun-(Earth+Moon) masses. Both the Sun and the Earth+Moon are assumed to be point masses and their motion is described by a circular orbit around their center of mass. In Eq. [1], $\bar{V}(x,y,z)$ is the total potential;

$$\bar{V}(x,y,z) = \frac{1}{2}(x^2+y^2) + \frac{\mu_1}{r_{1p}} + \frac{\mu_2}{r_{2p}} \quad [2]$$

which includes the potential effects of the rotating system (first term in the right-hand side) and the Sun and the Earth+Moon gravitation with normalised angular velocity, ω_0, equal to 1. When the effect of the Sun radiation is included, the SRP acts as a repulsive force with respect to the Sun's gravitational force (18, 19). a_x^s, a_y^s and a_z^s in Eq. [1] represent the SRP acceleration components of $\boldsymbol{a}^s$

$$\boldsymbol{a}^s = \beta\frac{\mu_1}{r_{1p}^2}\cdot\left\langle\frac{\boldsymbol{r}_{1p}}{|\boldsymbol{r}_{1p}|},\ \hat{\boldsymbol{N}}\right\rangle^2\cdot\hat{\boldsymbol{N}} \quad [3]$$

where, β is the lightness parameter that assumes values from 0 (no SRP effect) to 1 (SRP force is equal to the Sun gravitational force [1]). The lightness parameter, $\beta = \sigma^*/\sigma$, is a function of the mass-to-area ratio, σ, and the sun luminosity, $\sigma^* = 1.53\ g/m^2$ (20). $\hat{\boldsymbol{N}}$ is the normal to the reflective surface and it is defined as:

$$\hat{\boldsymbol{N}} = \begin{Bmatrix} cos(\Phi+\alpha)\cdot cos(\Psi+\delta) \\ sin(\Phi+\alpha)\cdot cos(\Psi+\delta) \\ sin(\Psi+\delta) \end{Bmatrix} \quad [4]$$

where, the angles Φ and Ψ describe the spacecraft-Sun vector with respect to the rotating system $\{x,\ y,\ z\}$. α and δ are the angles between the spacecraft-Sun vector and $\hat{\boldsymbol{N}}$ projected to the $x-y$ plane and $y-z$ plane, respectively, and they can assume values between $-\pi/2$ and $\pi/2$ (21, 22).

In Eq. [2-3], r_{1p} and r_{2p} are defined as:

$$r_{1p} = \sqrt{(x-x_1)^2+y^2+z^2} \quad [5]$$

$$r_{2p} = \sqrt{(x-x_2)^2+y^2+z^2} \quad [6]$$

where, $x_1 = -\mu$ is the position of the larger primary (i.e., Sun) and $x_2 = 1-\mu$ is the position of the smaller primary (i.e., Earth+Moon); moreover, the unit masses of the primaries are defined as $\mu_2 = \mu$ and $\mu_1 = 1-\mu$. For the Sun-(Earth+Moon) model, the value of μ which is the mass parameter of the system is $3.040147350673953\cdot10^{-6}$ in non-dimensional units.

Equation [1] refers to the general case; however, for a planar case, only the first two equations in Eq. [1] hold and their dependence to the z components is cancelled. If the SRP is not included in the model, then the dependence to

[1] $\beta = 1$ is just a theoretical value, not achievable for real applications.

a_x^s, a_y^s and a_z^s is cancelled. Finally, there are special cases in which the SRP is included in the system, but its effect is zero and it occurs when $\frac{\boldsymbol{r}_{1p}}{|\boldsymbol{r}_{1p}|}$ and $\hat{\boldsymbol{N}}$ are perpendicular vectors, in other words, when α or δ are equal to $\pm\pi/2$.

III FEEDBACK CONTROL OF THE NON-LINEAR SYSTEM

In a previous work, the Hamiltonian-Structure Preserving control was compared with the Floquét mode approach (12). By giving a high initial injection error due to failure in the halo insertion manoeuvre, it was possible to verify the robustness of the two methods by comparing their performances. First of all, the HSP shows to be robust when failure in the halo insertion manoeuvre occur while the FM not always converges. As already proved by Scheeres et al. (13), the HSP works also in a regime on non-linearities. Moreover, the advantages of HSP are that only an estimation of the state position error is needed, it is robust, the control does not depend on the selected orbit as for FM and the continuous acceleration required is very small (the over all ΔV is less if compared with the FM requirements). These suggest that HSP is preferable for low-thrust applications or, when possible, for propellant-free systems that exploit SRP. In our opinion, the advantage of HSP is in exploiting the natural dynamics of the restricted three-body problem to stabilise the motion of the spacecraft and it shows to be a promising approach. Thus, this work, shows how the extended HSP control law was derived for high-amplitude orbits, how to select the gain of the improved control law and, it is also investigated when SRP can be exploited for the orbit control.

III.I Design of the control law that preserve the Hamiltonian structure of the system

The Hamiltonian Structure-Preserving control uses the eigenstructure of the linearised equations of motion to design the control law. As shown by Scheeres et al. (13), this controller aims to remove both the stable and unstable manifolds by projecting the state position error (between the current and the target orbit) along their directions. This creates an artificial center manifold that keeps the trajectory close to the target orbit, as the poles of the linearised dynamics are placed along the imaginary axis. This creates a local stability that impacts onto the periodic orbit stability by affecting the eigenvalues of the monodromy matrix $\boldsymbol{M}$ that is the state transitional matrix of the system evaluated after one orbital period $\boldsymbol{\Phi}(P, t_0)$. For Lyapunov stability, the controller should place the eigenvalues of $\boldsymbol{M}$ on the unitary circle of the complex plane (23), (see figure 1). Thanks to the effect

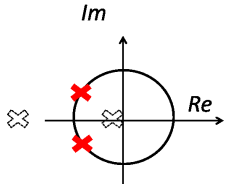

Figure 1: Eigenvalues of the monodromy matrix with (red crosses) and without (white crosses) the effect of the HSP controller.

of the control, the matrix $\boldsymbol{M}$ is still sympletic, since the two pairs of eigenvectors are the inverse of each other, but the existence of a Jacoby integral is no longer guaranteed since the central two real solutions equal to one are removed. Moreover, the fact that the monodromy matrix is symplectic guarantees also that the system is still autonomous and Hamiltonian (13). Scheeres demonstrated that the study of local stability is connected to the periodic orbit stability. Given a reference trajectory $\bar{\boldsymbol{X}}(t)$ going from an initial state $\bar{\boldsymbol{X}}_0$ to a final state $\bar{\boldsymbol{X}}_f$ under the effect of the natural dynamics in Eq. [1] written in a compact form as

$$\dot{\boldsymbol{X}} = f(\boldsymbol{X}), \qquad [7]$$

the State Transition Matrix (STM) can be computed as

$$\dot{\boldsymbol{\Phi}}(t, t_0) = \boldsymbol{Df}(\bar{\boldsymbol{X}}(t)) \cdot \boldsymbol{\Phi}(t, t_0), \qquad [8]$$

with $\boldsymbol{\Phi}(t_0, t_0) = \boldsymbol{I}$. Where, $\boldsymbol{Df}(\bar{\boldsymbol{X}}(t))$ is the Jacobian matrix of the flow field f evaluated along the reference trajectory. The variational equations are:

$$\delta\dot{\bar{\boldsymbol{X}}}(t) = \boldsymbol{Df}(\bar{\boldsymbol{X}}(t))\delta\bar{\boldsymbol{X}}(t) \qquad [9]$$

which are the linearised equations for the evaluation of variations $\delta\bar{\boldsymbol{X}}(t)$. Indeed, for the linearised equations, solving the eigenvalues of the variational equations matrix, $\boldsymbol{Df}(\bar{\boldsymbol{X}}(t))$, is an approximation of solving the eigenvalues problem of the STM, $\boldsymbol{\Phi}(t,t_0)$. The variational equations of Eq. [1] are;

$$\frac{d}{dt}\begin{bmatrix}\delta\boldsymbol{r}\\ \delta\dot{\boldsymbol{r}}\end{bmatrix}=\begin{bmatrix}\boldsymbol{0} & \boldsymbol{I}\\ \bar{\boldsymbol{V}}_{\boldsymbol{rr}} & 2\omega_0\boldsymbol{J}\end{bmatrix}\begin{bmatrix}\delta\boldsymbol{r}\\ \delta\dot{\boldsymbol{r}}\end{bmatrix} \quad [10]$$

$$\boldsymbol{J}=\begin{bmatrix}0 & 1\\ -1 & 0\end{bmatrix} \quad [11]$$

where, $\bar{\boldsymbol{V}}_{\boldsymbol{rr}}$ is the Jacobian matrix of the potential acceleration in Eq. [2], $2\omega_0\boldsymbol{J}$ is the term associated to the Coriolis acceleration. In Eq. [10], $\delta\boldsymbol{r}$ and $\delta\dot{\boldsymbol{r}}$ are the state position and velocity errors, respectively. The eigenvalues of the linearised dynamics are the solutions of the characteristic equations $D(\lambda)=|\boldsymbol{Df}-\lambda\boldsymbol{I}|=0$, where the characteristic polynomial is:

$$\Lambda^2+b\Lambda+c=0 \quad [12]$$

$$\begin{cases} b=4\omega_0^2-\bar{V}_{xx}-\bar{V}_{yy}\\ c=\bar{V}_{xx}\bar{V}_{yy}-\bar{V}_{xy}^2\\ \Delta=b^2-4c\end{cases}. \quad [13]$$

The solutions of Eq. [12] are affected by the sign of Δ. When, $\Delta>0$ the system admits two real and unequal roots; while, when $\Delta<0$ there are two complex and conjugate solutions. This fact is evident for high amplitude orbits where it is possible to identify two cases along the trajectory where the eigenvalues are couples of real and pure imaginary numbers (saddle×center equilibrium, i.e., the black line in Figure 2-3, when $b<0$, $\Delta>0$ and $c<0$), or where the eigenvalues are a couples of complex numbers and conjugate pairs (stable×unstable foci, i.e., the red line in Figure 2-3, when $b<0$, $\Delta<0$ and $c<0$).

The general solution of Eq. [12] is given by:

$$\Lambda_1=\lambda_{1,2}^2=\frac{-b+\sqrt{\Delta}}{2} \quad [14]$$

$$\Lambda_2=\lambda_{3,4}^2=\frac{-b-\sqrt{\Delta}}{2} \quad [15]$$

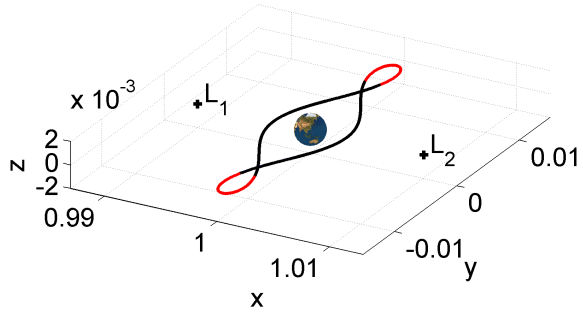

Figure 2: DPO and eigenvalues along the orbit where the black arc denotes the hyperbolic×center solutions and the red arc represents couples of complex and conjugate solutions (the Earth is not in scale).

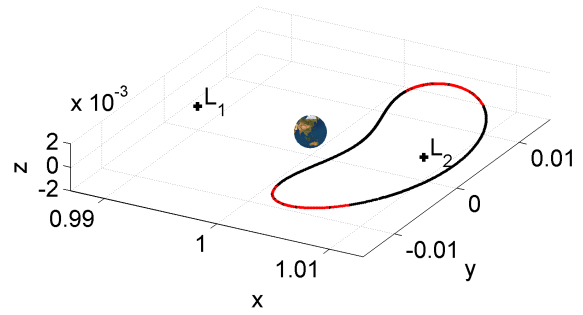

Figure 3: Planar-Lyapunov and eigenvalues along the orbit where the black arc denotes the hyperbolic×center solutions and the red arc represents couples of complex and conjugate solutions (the Earth is not in scale).

$$\widehat{\boldsymbol{x}}_k=\left\{\begin{array}{c}1\\ u_k\\ \lambda_k\\ \lambda_k\cdot u_k\end{array}\right\}; \quad [16]$$

where, λ_k are the eigenvalues and $\widehat{\boldsymbol{x}}_k$ their corresponding eigenvectors for k varying from 1 to 4. The HSP aims to project the state position error along the eigenvectors direction. From a vecto-

rial point of view, it is like defining a projection tensor given by $\boldsymbol{u}_k\boldsymbol{u}_k^T$ (13). The first two normalised components of $\widehat{\boldsymbol{x}}_k$ in Eq. [14] represent the unitary vector $\boldsymbol{u}_k$, and the expression of $\boldsymbol{u}_k$ is:

$$\boldsymbol{u}_k = \frac{1}{\sqrt{1+u_k\bar{u}_k}}\begin{bmatrix} 1 \\ u_k \end{bmatrix} \quad u_k = \frac{\lambda_k^2 - \bar{V}_{xx}}{\bar{V}_{xy} + 2\omega_0\lambda_k} \qquad [17]$$

where, $u_k\bar{u}_k$ is the product of u_k and its conjugate. Since the HSP control aims to stabilise the system in the sense of Lyapunov, the control law is designed such as to affect the sign of b, c and Δ of Eq. [12]. Indeed, the simple Lyapunov stability can be achieved by placing the eigenvalues of the linearised dynamics, the poles, on the imaginary axis, Figure 4, by adding to $\bar{\boldsymbol{V}}_{\boldsymbol{rr}}$ an artificial potential, the center manifold $\boldsymbol{T}$.

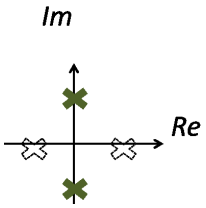

Figure 4: Eigenvalues of the linearised dynamics with (green crosses) and without (white crosses) the effect of the HSP controller.

The artificial center manifold, $\boldsymbol{T}$, is constructed from the linear combination of the projection tensors $\boldsymbol{u}_k\boldsymbol{u}_k^T$ and the gains. This linear combination is selected such as $\tilde{b}$, $\tilde{c}$ and $\tilde{\Delta}$, which are the indexes of stability affected by the control law, are all major than zero (13). $\{\tilde{b} > 0 \;\&\; \tilde{c} > 0 \;\&\; \tilde{\Delta} > 0\}$ is the condition of simple Lyapunov stability where the HSP control is added to the dynamics in Eq. [1] as an additional acceleration $\boldsymbol{T_c}$ obtained by multiplying $\boldsymbol{T}$ by the state position error between the target orbit and the actual spacecraft trajectory $\delta\boldsymbol{r}$,

$$\boldsymbol{T_c} = \boldsymbol{T}\delta\boldsymbol{r}. \qquad [18]$$

The acceleration, $\boldsymbol{T_c}$, affects the linearised dynamics and $\boldsymbol{Df}(\bar{\boldsymbol{X}}(t))$, in Eq. [10], turns into $\boldsymbol{Df_c}(\bar{\boldsymbol{X}}(t))$:

$$\boldsymbol{Df}_c(\bar{\boldsymbol{X}}(t)) = \begin{bmatrix} \boldsymbol{0} & \boldsymbol{I} \\ \bar{\boldsymbol{V}}_{\boldsymbol{rr}} & 2\omega_0\boldsymbol{J} \end{bmatrix}. \qquad [19]$$

The effect of the controller modifies $\bar{\boldsymbol{V}}_{\boldsymbol{rr}}$ into $\tilde{\boldsymbol{V}}_{\boldsymbol{rr}}$ as:

$$\tilde{\boldsymbol{V}}_{\boldsymbol{rr}} = \bar{\boldsymbol{V}}_{\boldsymbol{rr}} + \boldsymbol{T}. \qquad [20]$$

In this work, the full formulation of the proposed extended HSP controller is derived. The control law proposed by Scheeres et al. (13) is used when there is an hyperbolic×center equilibrium ($\Delta > 0$) which is summarised in Section III.I.1. Besides, in case of couples of complex and conjugate solutions ($\Delta < 0$), the dynamics presents a modified control law proposed in Section III.I.2.

III.I.1 Control law for hyperbolic×center equilibrium

In this section the control law proposed by Scheeres et al. (13) is summarised since this control law is used in case of hyperbolic×center equilibrium (see Figure 5).

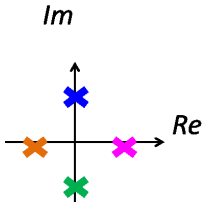

Figure 5: Couples of real and pure imaginary eigenvalues of the linearised equations: λ_1 (magenta cross), λ_2 (orange cross), λ_3 (blue cross) and λ_4 (green cross).

Moreover, it is useful to compare this formulation with the proposed control law for complex and conjugate roots (in Section III.I.2) in order to understand the main differences. The hyperbolic characteristic exponents for the stable (λ_1) and unstable (λ_2) directions are the solutions of the linearised dynamics in Eq. [14] where now the real roots $\lambda_{1,2}$ are named as $\pm\sigma$. The corresponding eigenvector to σ is:

$$\boldsymbol{u}_1 = \frac{1}{\sqrt{1+u_1^2}}\begin{bmatrix} 1 \\ u_1 \end{bmatrix} \quad u_1 = \frac{\sigma^2 - \bar{V}_{xx}}{\bar{V}_{xy} + 2\omega_0\sigma}; \qquad [21]$$

where, u_1 is real and such that the projection tensor $\boldsymbol{u}_1\boldsymbol{u}_1^T$

$$\boldsymbol{u}_1\boldsymbol{u}_1^T = \frac{1}{1+u_1^2}\begin{bmatrix} 1 & u_1 \\ u_1 & u_1^2 \end{bmatrix} \quad [22]$$

is real. The corresponding eigenvector to $-\sigma$ is, instead:

$$\boldsymbol{u}_2 = \frac{1}{\sqrt{1+u_2^2}}\begin{bmatrix} 1 \\ u_2 \end{bmatrix} \quad u_2 = \frac{\sigma^2 - \bar{V}_{xx}}{\bar{V}_{xy} - 2\omega_0\sigma}; \quad [23]$$

where, u_2 is real and the projection tensor $\boldsymbol{u}_2\boldsymbol{u}_2^T$

$$\boldsymbol{u}_2\boldsymbol{u}_2^T = \frac{1}{1+u_2^2}\begin{bmatrix} 1 & u_2 \\ u_2 & u_2^2 \end{bmatrix} \quad [24]$$

is real. The control law proposed by Scheeres et al. (13) is:

$$\boldsymbol{T_c} = -\sigma^2 G_1 \left[\boldsymbol{u}_1\boldsymbol{u}_1^T + \boldsymbol{u}_2\boldsymbol{u}_2^T\right]\delta\boldsymbol{r}. \quad [25]$$

As said, the control law validity in Eq. [25] is for solutions where the instantaneous map has two couples of real and pure imaginary eigenvalues.

III.I.2 Control law for complex and conjugate pairs

When couples of complex and conjugate numbers occur, the eigenvalues are the solution of the linear system in Eq. [14], where now $\lambda_{1,2,3,4}$ are complex and conjugate pairs; thus now $\lambda_{1,2}$ and $\lambda_{3,4}$ are $\pm(\sigma+\gamma i)$ and $\pm(\sigma-\gamma i)$ respectively, (Figure 6). The idea behind the design of the extended control law is to get rid of the imaginary components in order to have a real control acceleration. Thus, the eigenvectors component are separately analysed, in order to highlight possible conjugate terms for the design of the eigenvectors normalisation and the control acceleration. Starting form $\lambda_1 = \sigma + \gamma i$, its correspondent eigenvector component u_1 is:

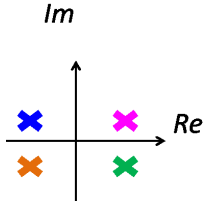

Figure 6: Couples of complex an conjugate eigenvalues of the linearised equations: λ_1 (magenta cross), λ_2 (orange cross), λ_3 (green cross) and λ_4 (blue cross).

$$u_1 = \frac{\sigma^2 - \bar{V}_{xx} - \gamma^2 + 2\sigma\gamma i}{\bar{V}_{xy} + 2\omega_0\sigma + 2\omega_0\gamma i}. \quad [26]$$

The complex nature of the eigenvector is highlighted as,

$$u_1 = \frac{A_1 + B_1 i}{C_1 + D_1 i}, \quad [27]$$

that, after mathematical manipulation, can be written as:

$$u_1 = \frac{(A_1C_1 + B_1D_1) - (A_1D_1 - B_1C_1)i}{C_1^2 + D_1^2} \quad [28]$$

where,

$$\begin{cases} A_1 = \sigma^2 - \bar{V}_{xx} - \gamma^2 \\ B_1 = 2\sigma\gamma \\ C_1 = \bar{V}_{xy} + 2\omega_0\sigma \\ D_1 = 2\omega_0\gamma \end{cases}. \quad [29]$$

The same approach can be use for $\lambda_2 = -\sigma - \gamma i$; where, the correspondent eigenvector component is defined as

$$u_2 = \frac{\sigma^2 - \bar{V}_{xx} - \gamma^2 + 2\sigma\gamma i}{\bar{V}_{xy} - 2\omega_0\sigma - 2\omega_0\gamma i} \quad [30]$$

that is a complex number,

$$u_2 = \frac{A_2 + B_2 i}{C_2 - D_2 i}. \quad [31]$$

Thus, it is possible to highlight the real and imaginary part of u_2 as

$$u_2 = \frac{(A_2C_2 - B_2D_2) + (A_2D_2 + B_2C_2)i}{C_2^2 + D_2^2} \quad [32]$$

where,

$$\begin{cases} A_2 = \sigma^2 - \bar{V}_{xx} - \gamma^2 \\ B_2 = 2\sigma\gamma \\ C_2 = \bar{V}_{xy} - 2\omega_0\sigma \\ D_2 = 2\omega_0\gamma \end{cases}. \quad [33]$$

As before, the correspondent eigenvector component u_3 to $\lambda_3 = \sigma - \gamma i$ is:

$$u_3 = \frac{\sigma^2 - \bar{V}_{xx} - \gamma^2 - 2\sigma\gamma i}{\bar{V}_{xy} + 2\omega_0\sigma - 2\omega_0\gamma i} \quad [34]$$

that has a complex nature too

$$u_3 = \frac{A_3 - B_3 i}{C_3 - D_3 i} \quad [35]$$

and, by manipulating the previous expression, it is possible to write:

$$u_3 = \frac{(A_3 C_3 + B_3 D_3) + (A_3 D_3 - B_3 C_3) i}{C_2^2 + D_2^2} \quad [36]$$

where,

$$\begin{cases} A_3 = \sigma^2 - \bar{V}_{xx} - \gamma^2 \\ B_3 = 2\sigma\gamma \\ C_3 = \bar{V}_{xy} + 2\omega_0\sigma \\ D_3 = 2\omega_0\gamma \end{cases} . \quad [37]$$

Finally, in the case of $\lambda_4 = -\sigma + \gamma i$, the correspondent eigenvector component is u_4,

$$u_4 = \frac{\sigma^2 - \bar{V}_{xx} - \gamma^2 - 2\sigma\gamma i}{\bar{V}_{xy} - 2\omega_0\sigma + 2\omega_0\gamma i}. \quad [38]$$

u_4 is a complex number and can be written as:

$$u_4 = \frac{A_4 - B_4 i}{C_4 + D_4 i} \quad [39]$$

and it can be defined also as:

$$u_4 = \frac{(A_4 C_4 - B_4 D_4) - (A_4 D_4 + B_4 C_4) i}{C_4^2 + D_4^2} \quad [40]$$

where,

$$\begin{cases} A_4 = \sigma^2 - \bar{V}_{xx} - \gamma^2 \\ B_4 = 2\sigma\gamma \\ C_4 = \bar{V}_{xy} - 2\omega_0\sigma \\ D_4 = 2\omega_0\gamma \end{cases} . \quad [41]$$

By noticing that

$$\begin{cases} A_1 = A_2 = A_3 = A_4 = A = \sigma^2 - \bar{V}_{xx} - \gamma^2 \\ B_1 = B_2 = B_3 = B_4 = B = 2\sigma\gamma \\ C_1 = C_3 = C = \bar{V}_{xy} + 2\omega_0\sigma \\ C_2 = C_4 = \bar{C} = \bar{V}_{xy} - 2\omega_0\sigma \\ D_1 = D_2 = D_3 = D_4 = D = 2\omega_0\gamma \end{cases} , \quad [42]$$

it is possible to rewrite the expression of u_k, with k defined from 1 to 4, as:

$$u_1 = \frac{(AC + BD) - (AD - BC) i}{C^2 + D^2} \quad [43]$$

$$u_2 = \frac{(A\bar{C} - BD) + (AD + B\bar{C}) i}{\bar{C}^2 + D^2} \quad [44]$$

$$u_3 = \frac{(AC + BD) + (AD - BC) i}{C^2 + D^2} \quad [45]$$

$$u_4 = \frac{(A\bar{C} - BD) - (AD + B\bar{C}) i}{\bar{C}^2 + D^2}. \quad [46]$$

Moreover, if a change of variables is applied,

$$\begin{cases} \bar{a} = AC + BD \\ \bar{b} = AD - BC \\ \bar{c} = C^2 + D^2 \\ \bar{d} = A\bar{C} - BD \\ \bar{e} = AD + B\bar{C} \\ \bar{f} = \bar{C}^2 + D^2 \end{cases} , \quad [47]$$

it is possible to define the eigenvectors and their normalisations by knowing that u_3 is the conjugate of u_1 and u_4 is the conjugate of u_2:

$$\boldsymbol{u_1} = \frac{1}{\sqrt{1 + u_1 u_3}} \begin{bmatrix} 1 \\ u_1 \end{bmatrix} \quad u_1 = \frac{\bar{a} - \bar{b} i}{\bar{c}} \quad [48]$$

$$\boldsymbol{u_3} = \frac{1}{\sqrt{1 + u_1 u_3}} \begin{bmatrix} 1 \\ u_3 \end{bmatrix} \quad u_3 = \frac{\bar{a} + \bar{b} i}{\bar{c}} \quad [49]$$

$$\boldsymbol{u_2} = \frac{1}{\sqrt{1 + u_2 u_4}} \begin{bmatrix} 1 \\ u_2 \end{bmatrix} \quad u_2 = \frac{\bar{d} + \bar{e} i}{\bar{f}} \quad [50]$$

$$\boldsymbol{u_4} = \frac{1}{\sqrt{1 + u_2 u_4}} \begin{bmatrix} 1 \\ u_4 \end{bmatrix} \quad u_4 = \frac{\bar{d} - \bar{e} i}{\bar{f}} \quad [51]$$

where, $\bar{a}$, $\bar{b}$, $\bar{c}$, $\bar{d}$, $\bar{e}$ and $\bar{f}$ are functions of the eigenvalues and $\bar{\boldsymbol{V}}_{\boldsymbol{rr}}$:

$$\begin{cases} \bar{a} = (\sigma^2 - \bar{V}_{xx} - \gamma^2)(\bar{V}_{xy} + 2\omega_0\sigma) + (2\sigma\gamma)(2\omega_0\gamma) \\ \bar{b} = (\sigma^2 - \bar{V}_{xx} - \gamma^2)(2\omega_0\gamma) - (2\sigma\gamma)(\bar{V}_{xy} + 2\omega_0\sigma) \\ \bar{c} = (\bar{V}_{xy} + 2\omega_0\sigma)^2 + (2\omega_0\gamma)^2 \\ \bar{d} = (\sigma^2 - \bar{V}_{xx} - \gamma^2)(\bar{V}_{xy} - 2\omega_0\sigma) - (2\sigma\gamma)(2\omega_0\gamma) \\ \bar{e} = (\sigma^2 - \bar{V}_{xx} - \gamma^2)(2\omega_0\gamma) + (2\sigma\gamma)(\bar{V}_{xy} - 2\omega_0\sigma) \\ \bar{f} = (\bar{V}_{xy} - 2\omega_0\sigma)^2 + (2\omega_0\gamma)^2 \end{cases} . \quad [52]$$

Since u_1 and u_3 are complex conjugate and u_2 and u_4 are complex and conjugate, we can write a new control law as follow. From the normalisation we know that:

$$u_1 u_3 = (\bar{a} - \bar{b} i) \cdot (\bar{a} + \bar{b} i) = \bar{a}^2 + \bar{b}^2 \quad [53]$$

$$u_2 u_4 = (\bar{d} + \bar{e} i) \cdot (\bar{d} - \bar{e} i) = \bar{d}^2 + \bar{e}^2. \quad [54]$$

The four projection tensors are defined as:

$$\boldsymbol{u_1}\boldsymbol{u_1}^T = \frac{1}{1+u_1u_3}\begin{bmatrix} 1 & u_1 \\ u_1 & u_1^2 \end{bmatrix} \quad [55]$$

$$\boldsymbol{u_3}\boldsymbol{u_3}^T = \frac{1}{1+u_1u_3}\begin{bmatrix} 1 & u_3 \\ u_3 & u_3^2 \end{bmatrix} \quad [56]$$

$$\boldsymbol{u_2}\boldsymbol{u_2}^T = \frac{1}{1+u_2u_4}\begin{bmatrix} 1 & u_2 \\ u_2 & u_2^2 \end{bmatrix} \quad [57]$$

$$\boldsymbol{u_4}\boldsymbol{u_4}^T = \frac{1}{1+u_2u_4}\begin{bmatrix} 1 & u_4 \\ u_4 & u_4^2 \end{bmatrix}. \quad [58]$$

It is interesting to note that the only linear combination among the projection tensors, that guarantee a real control law, requires couple of projection tensors to be weighted with the same gain. This can be demonstrate by looking at $\boldsymbol{u}_k$ and u_k in Eq. [48-51], the only solution is to keep the tensors associate to $\boldsymbol{u_1}$ and $\boldsymbol{u_3}$ with the same gain such as:

$$\boldsymbol{u_1}\boldsymbol{u_1}^T+\boldsymbol{u_3}\boldsymbol{u_3}^T = \frac{1}{1+u_1u_3}\begin{bmatrix} 1 & u_1+u_3 \\ u_1+u_3 & u_1^2+u_3^2 \end{bmatrix}, \quad [59]$$

$$u_1+u_3 = \bar{a}-\bar{b}i+\bar{a}+\bar{b}i = 2\bar{a} \quad [60]$$

and

$$u_1^2+u_3^2 = (\bar{a}-\bar{b}i)^2+(\bar{a}+\bar{b}i)^2 = 2(\bar{a}^2-\bar{b}^2) \quad [61]$$

are all real. For the same reason, the tensors associated to $\boldsymbol{u_2}$ and $\boldsymbol{u_4}$ should be weighted with the same gain to achieve a real control acceleration. Indeed,

$$\boldsymbol{u_2}\boldsymbol{u_2}^T+\boldsymbol{u_4}\boldsymbol{u_4}^T = \frac{1}{1+u_2u_4}\begin{bmatrix} 1 & u_2+u_4 \\ u_2+u_4 & u_2^2+u_4^2 \end{bmatrix}, \quad [62]$$

$$u_2+u_4 = \bar{d}+\bar{e}i+\bar{d}-\bar{e}i = 2\bar{d} \quad [63]$$

and

$$u_2^2+u_4^2 = (\bar{d}+\bar{e}i)^2+(\bar{d}-\bar{e}i)^2 = 2(\bar{d}^2-\bar{e}^2) \quad [64]$$

are real terms too. The proposed control law for couples of complex and conjugate pairs weights with the same gain couples of complex and conjugate eigenvectors, in order to have a real control acceleration and to cancel the imaginary parts out:

$$\boldsymbol{T_c} = \{ \begin{array}{l} -\lambda_1\lambda_3 G_1\left[\boldsymbol{u_1}\boldsymbol{u_1}^T+\boldsymbol{u_3}\boldsymbol{u_3}^T\right] \\ -\lambda_2\lambda_4 G_2\left[\boldsymbol{u_2}\boldsymbol{u_2}^T+\boldsymbol{u_4}\boldsymbol{u_4}^T\right]\end{array}\} \delta\boldsymbol{r} \quad [65]$$

where,

$$\lambda_1\lambda_3 = (\sigma+\gamma i)(\sigma-\gamma i) = \sigma^2+\gamma^2 \quad [66]$$

and

$$\lambda_2\lambda_4 = (-\sigma-\gamma i)(-\sigma+\gamma i) = \sigma^2+\gamma^2 \quad [67]$$

are real and positive numbers. Thus, $\boldsymbol{T_c}$ can be further simplified to:

$$\boldsymbol{T_c} = -\left(\sigma^2+\gamma^2\right) \begin{array}{l}\{G_2\left[\boldsymbol{u_1}\boldsymbol{u_1}^T+\boldsymbol{u_3}\boldsymbol{u_3}^T\right] \\ +G_3\left[\boldsymbol{u_2}\boldsymbol{u_2}^T+\boldsymbol{u_4}\boldsymbol{u_4}^T\right]\delta\boldsymbol{r}.\end{array} \quad [68]$$

In conclusion, the HSP control algorithm is designed such as:

$$\boldsymbol{T_c} = \begin{cases} \text{Equation [25]} & \text{if } \Delta > 0 \\ \text{Equation [68]} & \text{if } \Delta < 0. \end{cases} \quad [69]$$

The proposed control in Eq. [69] was implemented in the CRUISE (Controlled Routes by Using Innovative Solar-radiation Equipments) algorithm in Matlab language. An important remark is that not all the gain sets (G_1, G_2 and G_3) can stabilise the orbit, since the local stability is not a necessary condition of the periodic orbit stability due to resonance effects (13).

IV GAIN DEFINITION TO ACHIEVE SIMPLE LYAPUNOV STABILITY

The simple stability is guaranteed for:

$$\begin{cases} \tilde{b} = 4\omega^2-\tilde{V}_{xx}-\tilde{V}_{yy} > 0 \\ \tilde{c} = \tilde{V}_{xx}\tilde{V}_{yy}-\tilde{V}_{xy}^2 > 0 \\ \tilde{\Delta} = \tilde{b}^2-4\tilde{c} > 0 \end{cases}. \quad [70]$$

The linear stability was already proved by Scheeres et al. (13) for the hyperbolic×center equilibrium; where, G_1 in Eq. [25] should be selected large enough to guarantee linear stability. In this section, a similar approach is used to study the characteristics of G_2 and G_3 of Eq. [68] to reach linear stability in the case of couples of complex and conjugate eigenvalues. For the definition of the control law in Eq. [68], $\tilde{V}_{xx}$, $\tilde{V}_{yy}$ and $\tilde{V}_{xy}$ are defined as:

$$\tilde{V}_{xx} = \bar{V}_{xx}-G_2\frac{(\sigma^2+\gamma^2)}{1+u_1u_3}-G_3\frac{(\sigma^2+\gamma^2)}{1+u_2u_4} \quad [71]$$

$$\tilde{V}_{yy} = \bar{V}_{yy} \quad -G_2\frac{(\sigma^2+\gamma^2)(u_1^2+u_3^2)}{1+u_1u_3} \quad -G_3\frac{(\sigma^2+\gamma^2)(u_2^2+u_4^2)}{1+u_2u_4} \quad [72]$$

$$\tilde{V}_{xy} = \bar{V}_{xy} \quad -G_2\frac{(\sigma^2+\gamma^2)(u_1+u_3)}{1+u_1u_3} \quad -G_3\frac{(\sigma^2+\gamma^2)(u_2+u_4)}{1+u_2u_4} \quad . \quad [73]$$

The definition of $\tilde{b}$ is:

$$\tilde{b} = b+(\sigma^2+\gamma^2)\left[G_2\frac{1+u_1^2+u_3^2}{1+u_1u_3} + G_3\frac{1+u_2^2+u_4^2}{1+u_4u_4}\right] \quad [74]$$

Since $b < 0$ and $\tilde{b}$ must be > 0, it is important to study the sign of the terms associated to the controller. In Eq. [74], $u_1u_3 = \bar{a}^2 + \bar{b}^2$ and $u_2u_4 = \bar{d}^2 + \bar{e}^2$ are positive terms, thus all the fractions are positive (> 0). This means that for the first condition in Eq. [70], G_2 and G_3 should be positive and big enough to keep $\tilde{b} > 0$. As a consequence of Eq. [70], $\tilde{b}^2$ must be $> 4\tilde{c}$ such as $\tilde{\Delta} > 0$. The definition of $\tilde{\Delta}$ is

$$\tilde{\Delta} = (4\omega^2 - \tilde{V}_{xx} - \tilde{V}_{yy})^2 - 4(\tilde{V}_{xx}\tilde{V}_{yy} - \tilde{V}_{xy}^2) \quad [75]$$

where, Eq. [75] can be rewritten as:

$$\tilde{\Delta} = 8\omega^2\tilde{b} + (\tilde{V}_{xx} - \tilde{V}_{yy})^2 + 4\tilde{V}_{xy}^2. \quad [76]$$

Since $(\tilde{V}_{xx} - \tilde{V}_{yy})^2$ and $\tilde{V}_{xy}^2$ are positive terms, the condition $\tilde{\Delta} > 0$ is satisfied by $\tilde{b} > 0$. The definition of $\tilde{c}$ is:

$$\tilde{c} = c \quad +(\sigma^2+\gamma^2)^2\left[G_2^2\frac{u_1^2+u_3^2}{(1+u_1u_3)^2} + G_3^2\frac{u_2^2+u_4^2}{(1+u_2u_4)^2} + \frac{G_2G_3(u_2^2+u_4^2+u_1^2+u_3^2)}{(1+u_2u_4)(1+u_1u_3)}\right] + K_n; \quad [77]$$

where, K_n are all the negative terms:

$$K_n = \quad -(\sigma^2+\gamma^2)\left\{G_2\left[\frac{\bar{V}_{xx}(u_1^2+u_3^2)+\bar{V}_{yy}}{1+u_1u_3} - \frac{2\bar{V}_{xy}(u_1+u_3)}{1+u_1u_3} + G_2(\sigma^2+\gamma^2)\frac{(u_1+u_3)^2}{(1+u_1u_3)^2}\right] + G_3\left[\frac{\bar{V}_{xx}(u_2^2+u_4^2)+\bar{V}_{yy}}{1+u_2u_4} - \frac{2\bar{V}_{xy}(u_2+u_4)}{1+u_2u_4} + G_3(\sigma^2+\gamma^2)\frac{(u_2+u_4)^2}{(1+u_2u_4)^2}\right] + 2G_2G_3(\sigma^2+\gamma^2)\frac{(u_1+u_3)(u_2+u_4)}{(1+u_2u_4)(1+u_1u_3)}\right\}. \quad [78]$$

Since $c < 0$, K_n collects all the negative terms and $\tilde{c}$ must be > 0, G_2 and G_3 must be positive and big enough to guarantee the stability. Note that from both $\tilde{b} > 0$ and $\tilde{c} > 0$ conditions, at least G_2 or G_3 must be different from zero.

V ARTIFICIAL POTENTIAL ENERGY

As previously mentioned, the effect of the HSP control is to add an artificial potential to the system to achieve simple Lyapunov stability. Thus in this section, we show the shape of the potential energy, (see Figure 7), and its double derivatives for the CRTBP planar dynamics. The double derivatives, Figures 8-10 light blue surfaces, of the potential function can be derived from Eq. [2] and the hypothesis of planar dynamics can be reached by simply setting $z = 0$ such as:

$$\bar{V}_{xx} = \omega^2 \quad -\frac{\mu_1}{r_{1p}^3}\frac{\left[1-(3(x-x_1)^2)\right]}{r_{1p}^2} \quad -\frac{\mu_2}{r_{2p}^3}\frac{\left[1-(3(x-x_2)^2)\right]}{r_{2p}^2} \quad [79]$$

$$\bar{V}_{yy} = \omega^2 - \frac{\mu_1}{r_{1p}^3}\frac{\left[1-(3y^2)\right]}{r_{1p}^2} - \frac{\mu_2}{r_{2p}^3}\frac{\left[1-(3y^2)\right]}{r_{2p}^2} \quad [80]$$

$$\bar{V}_{xy} = \frac{3\mu_1(x-x_1)y}{r_{1p}^5} + \frac{3\mu_2(x-x_2)y}{r_{2p}^5}. \quad [81]$$

For the case of hyperbolic×center equilibrium, the artificial potential matrix $\boldsymbol{T}$ is defined as in Eq. [25], where the double derivative artificial potential energy matrix is defined as $-\boldsymbol{T}$, see Figures 8-10 light green surfaces. Finally, the second derivatives of the modified potential are found by simply apply Eq. [20], where the correspondent modified potential energy is $\tilde{\boldsymbol{U}}_{\boldsymbol{rr}} = -\tilde{\boldsymbol{V}}_{\boldsymbol{rr}}$, Figures 11-13. Note that, all Figures in this section are obtained by fixing μ for the Sun-(Earth+Moon) system and $G_1 = 1$. Finally, in Figures 7-13 the dash black line is representative of the target orbit projected to the $x-y$ plane with $z = -1.5004$, which is the plane associated to the energy constant of the orbit (-1.500433040473652).

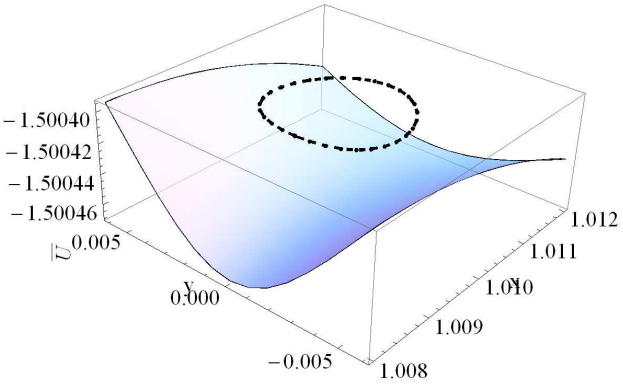

Figure 7: Potential energy: $\bar{U}(x, y) = -\bar{V}(x, y)$.

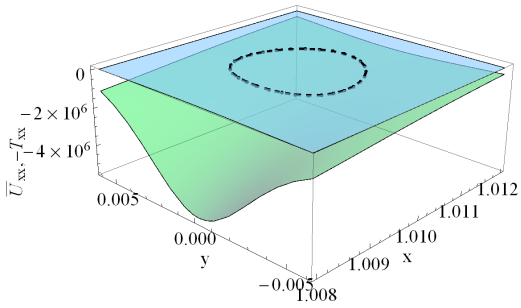

Figure 8: Second derivative in x of: the potential energy: $\bar{U}_{xx}(x, y) = -\bar{V}_{xx}(x, y)$ in light blue and the artificial potential energy $-T_{xx}(x, y)$ in green.

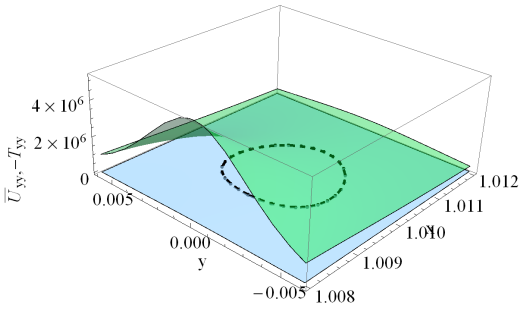

Figure 9: Second derivative in y of: the potential energy: $\bar{U}_{yy}(x, y) = -\bar{V}_{yy}(x, y)$ in light blue and the artificial potential energy $-T_{yy}(x, y)$ in green.

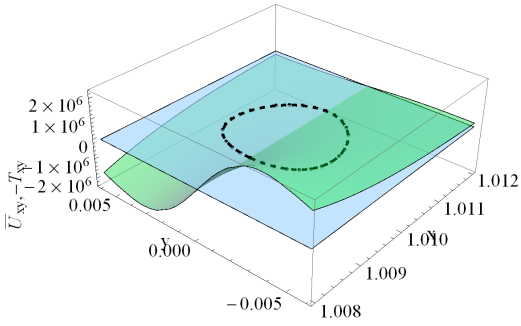

Figure 10: Second cross derivative in x and y of: the potential energy $\bar{U}_{xy}(x, y) = -\bar{V}_{xy}(x, y)$ in light blue and the artificial potential energy $-T_{xy}(x, y)$ in green.

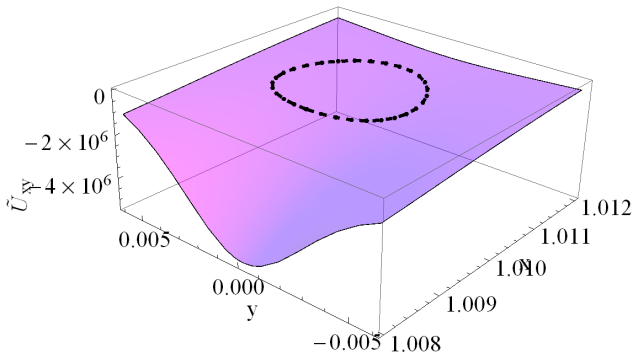

Figure 11: Second derivative in x of the modified potential energy: $\tilde{U}_{xx}(x, y)$.

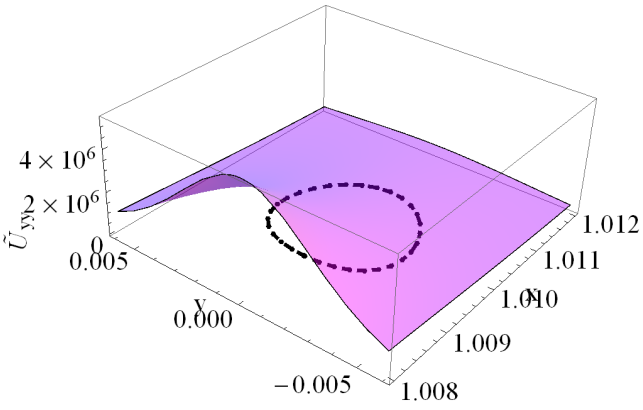

Figure 12: Second derivative in y of the modified potential energy: $\tilde{U}_{yy}(x, y)$.

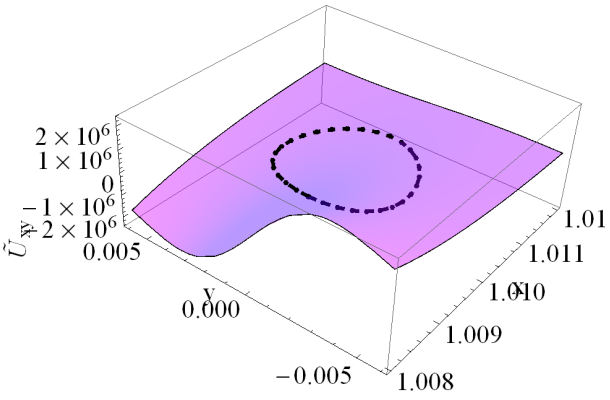

Figure 13: Second cross derivative in x and y of the modified potential energy: $\tilde{U}_{xy}(x, y)$.

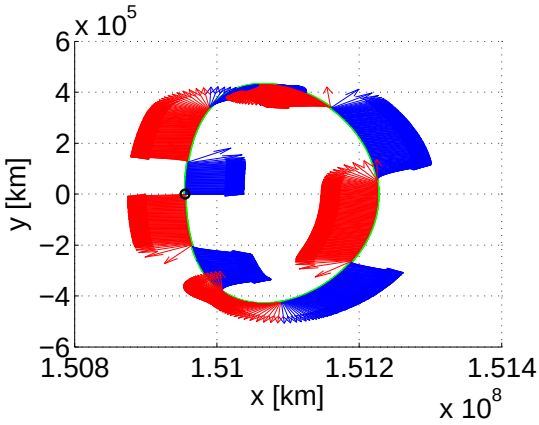

Figure 14: Direction of the control accelerations along the orbit: the blue arrows represent a feasible direction for SRP accelerations.

VI HSP CONTROL RESULTS

An exhaustive analysis of the HSP control law was performed in a previous work; where, the controller was applied for SOHO mission, DPOs and Planar-Lyapunov (12). The HSP control and its extended version to high-amplitude orbits guarantee the controllability of the orbits for a nominal mission of 5 year duration after the effects of failure in the halo insertion manoeuvre up to 10^5 km in position. However, the control of the orbits can be extended to a longer nominal mission by increasing the gains. For this study, it is selected a P-Lyapunov orbit in which an initial injection error of -40 km is applied. This orbit has all hyperbolic×center equilibria, (see Figure 14). Figure 14 shows that the controller keeps the trajectory closed to the target orbit in green; while, the red and blue arrows represent the directions of the control acceleration. As previously noticed (12), it is not always possible to apply SRP (red arrows in Figure 14) since the deployable reflective structures, the actuators, have a constrain in the orientation angle.

VII ACTUATORS MODEL: DEPLOYABLE REFLECTIVE STRUCTURES

In this section, the actuators model is presented and used to determine the reflective area and the orientation angles requirements from the control acceleration. The main idea is to consider SRP as the control acceleration; where, the vector direction determines the requirements in the area orientation angle. Instead, the size of the area is given from the module of the control acceleration. Note that the condition of a sun-pointing area is an ideal case since the area cross section is effectively used to control the spacecraft. On the other hand, when the orientation angles are close to the saturation point the requirement in the area will be higher since the effective projection area used is lower. The orientation of the reflective area should be limited not only between $-\pi/2$ and $+\pi/2$ but should be lower than that, in order to have a lower required area and to accomplish the spacecraft pointing requirements. The spacecraft-Sun direction is represented by Φ and Ψ,

$$\Phi = tan^{-1}\left(\frac{y}{x-\mu}\right) \qquad [82]$$

and

$$\Psi = tan^{-1}\left(\frac{z}{\sqrt{(x-\mu)^2+y^2}}\right). \qquad [83]$$

The normal vector to the reflective area can be derived as

$$\hat{\boldsymbol{N}} = \frac{\boldsymbol{T_c}}{|\boldsymbol{T_c}|} \qquad [84]$$

where, $\hat{\boldsymbol{N}}$ is given by Eq. [4]. In this way, the normal components can be found as:

$$\hat{N}_z = sin(\Psi + \delta) \quad \delta = sin^{-1}(\hat{N}_z) - \Psi \qquad [85]$$

and

$$\frac{\hat{N}_y}{\hat{N}_x} = tan(\Phi + \alpha) \quad \alpha = tan^{-1}(\frac{\hat{N}_y}{\hat{N}_x}) - \Phi. \quad [86]$$

Finally, the magnitude of the control acceleration is

$$\boldsymbol{T_c} = \beta \frac{(1-\mu)}{r_{1p}^2} \cdot \left\langle \frac{\boldsymbol{r}_{1p}}{|\boldsymbol{r}_{1p}|}, \hat{\boldsymbol{N}} \right\rangle^2 \left\{ \begin{array}{c} \hat{N}_x \\ \hat{N}_y \\ \hat{N}_z \end{array} \right\} \quad [87]$$

where,

$$|\boldsymbol{T_c}| = \beta \frac{(1-\mu)}{r_{1p}^2} \cdot \left\langle \frac{\boldsymbol{r}_{1p}}{|\boldsymbol{r}_{1p}|}, \hat{\boldsymbol{N}} \right\rangle^2. \quad [88]$$

Therefore, the required lightness parameter is

$$\beta = \frac{|\boldsymbol{T_c}| r_{1p}^2}{(1-\mu) \left\langle \frac{\boldsymbol{r}_{1p}}{|\boldsymbol{r}_{1p}|}, \hat{\boldsymbol{N}} \right\rangle^2}. \quad [89]$$

From Eq. [89], the area requirements can be found as:

$$A = \frac{\beta \cdot m}{\sigma^*}. \quad [90]$$

In Figure 15, it is shown the control acceleration required to stabilise the orbit; where, the orientation angle in Figure 16 is derived, from the control acceleration in Figure 15.

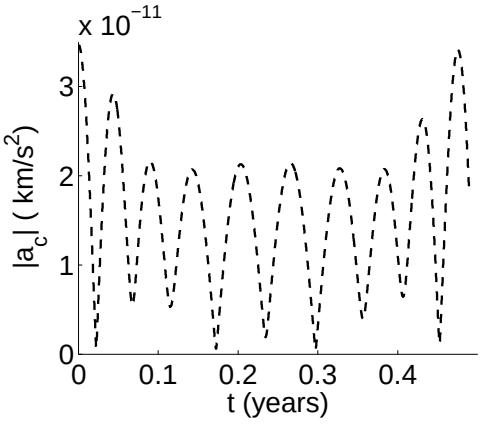

Figure 15: Threshold in the control acceleration after one orbital period.

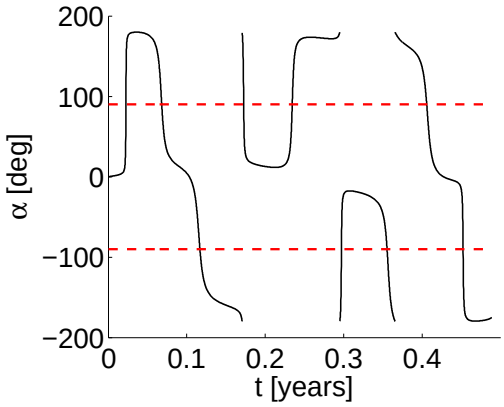

Figure 16: Requirements in the orientation angle after one orbital period.

VIII SATURATION OF THE ACTUATORS

When SRP is involved, in order to have a feasible acceleration, the control acceleration should never be sun-pointing (i.e. the spacecraft is escaping outwards from the Sun). Goméz et al. (24) named this peculiarity as the "always towards the Sun rule". This effect causes saturation in the actuator system as the reflective area orientation angle should be limited between $-\pi/2$ and $+\pi/2$. Gómez underlines that this effect cannot be overcome unless a very high area-to-mass ratio is used. A previous extension of HSP with SRP proposed by M. Xu and S. Xu (14) fulfilled the "always towards the Sun" rule by selecting a very high area-to-mass ratio to avoid saturation in the angles. Indeed, M. Xu and S. Xu (14) used an initial lightness parameter β_0 of 0.5059 which for a spacecraft with the same mass as SOHO corresponds to an initial area of $6.1270 \cdot 10^5$ m^2 which corresponds to a 782.75-m span of a squared area. Currently, JAXA's IKAROS mission demonstrates the capability to deploy a 20-m span sail (25); thus, this size of required area is unfeasible with current technology. Conversely, our study aims to minimise the area-to-mass ratio, thus an on/off control should be investigated to maintain a constant SRP effect, when the saturation occurs. Indeed, by simply switching off the control law, the saturation non-linearity of the actuators slows down the response of the feedback and thus causes the in-

tegrator state to "windup" to excessively large values, see Figure 17-18.

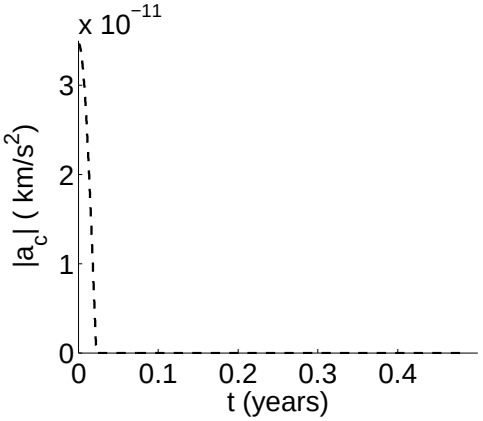

Figure 17: Windup in the control acceleration after switching off the controller.

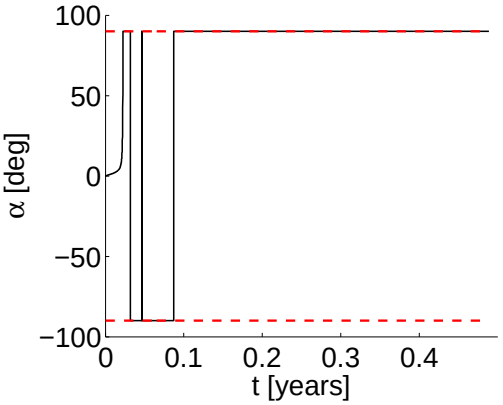

Figure 18: Wind up in the orientation angle after switching off the controller.

There are several possibilities to avoid saturation: one is to implement anti-windup schemes as for example nested saturations, direct linear anti-windup or model recovery anti-windup. The anti-windup refers to the augmentation of a controller in a feedback loop under windup conditions (16). Thus, acceptable performance is achieved even when actuator saturation occurs. Anti-windup methods may include also the redesign of the control law to include the effect of saturation directly in the control design. The last option should be considered when the control actuators are continuously trying to act beyond their limits. The nested saturation is a promising technique that was demonstrated to work well for feedback linearisation. The main idea is to defined a non-linear control law that is a non-linear combination of saturation functions of linear feedbacks. This allow to redesign the control law as non-linear and to include the constrains directly in the control law (17). However, it requires an exponentially stable plant and asymptotic stability of the unconstrained closed-loop control. Thus, due to the Hamiltonian nature of the controller and of the presence of an exponentially unstable mode, this method was discarded. A preliminary result in term of desired control solution with desaturation in the actuators is shown in Figure 19-22. However, with the current implementation, the controller under saturation can not guarantee stability for more then two orbital periods and during most of the time along the orbit the actuators are in saturations. Thus, there are several possibilities that might be pursued such as investigating other anti-windup algorithms, or redesigning the control law by including SRP and its actuators constrains. It was also investigated an hybrid control method that uses low-thrust engine where SRP is prohibited. A low-thrust system was compared with the hybrid combination of low-thrust and SRP devices for 4 years of mission. The amount of fuel consumed by low-thrust is 0.00728 [g] instead with the hybrid propulsion system the consumption is of 0.00354 [g]. Even if the amount of fuel saved is around 50%, in our opinion, the hybrid propulsion system should be discarded since low-thrust has already a low fuel expenditure. Thus, having a complex propulsion system that combines low-thrust with SRP is not a feasible choice. Therefore, the desaturation of the actuators will be further investigated and applied in a future work.

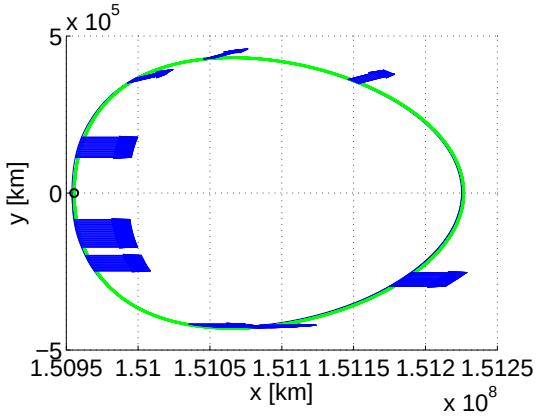

Figure 19: Desaturation of the control acceleration.

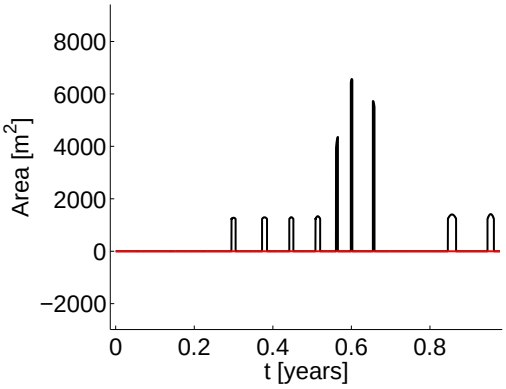

Figure 22: Required area due to the constrains in the orientation angle.

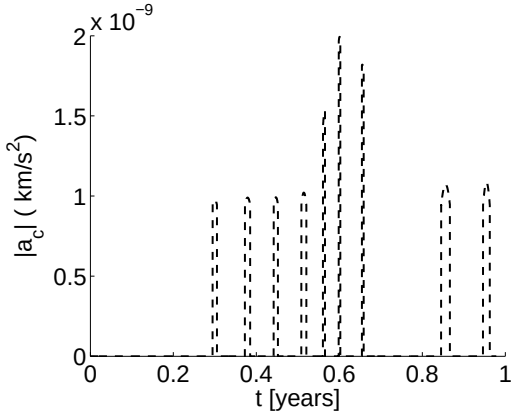

Figure 20: Low-thrust acceleration required when the saturation occurs.

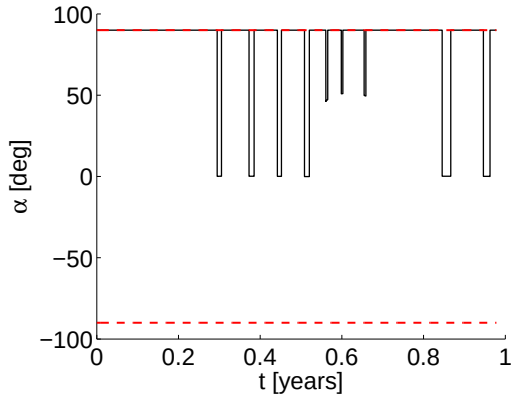

Figure 21: Constrained orientation angle.

IX CONCLUSIONS

In this paper, an extended version of the Hamiltonian structure preserving control for high amplitude orbit of the restricted three-body problem was presented. The condition of control stability determined how to select the set of gains. The effect of the controller onto the potential energy of the system was then analysed by showing the structure of the double derivative of the artificial centred manifold due to the effect of the control. Finally, the model of the actuators for Hamiltonian structure preserving enhanced by solar radiation pressure was shown with preliminary considerations on the effect of the control saturations.

References

(1) E. Perozzi and S. Ferraz-Mello. Space manifold dynamics. *Springer*, doi: 10.1007/978-1-4419-0348-8-1.

(2) J. P. Olive, T. V. Overbeek, and B. Fleck. Soho monthly trending report. *SOHO/PRG/TR/769 Oct 15*, 2013.

(3) R. Bauske. Operational manoeuvre optimization for the esa missions herschel and planck. *International Symposium on Space Flight Dynamics*, 2009.

(4) M. Hechler and J. Cobos. Herschel, planck and gaia orbit design. *7th International Conference on Libration Point Orbits and Application*, Parador d'Aiguablava, Girona, Spain, 10-14 June, 2002.

(5) E. Canalias, G. Gómez, M. Marcote, and J.J. Masdemont. Assessment of mission design including utilization of libration points and weak stability boundaries. *Ariadna id: 03/4103*, 2004.

(6) M. Hénon. Numerical exploration of the restricted problem. v. *Astron. and Astrophys.*, 1:223–238, 1968.

(7) M. Lara and R. Russell. Concerning the family g of the restricted three-body problem. *IX Jornadas de Trabajo en Mecanica Celeste*, 2006.

(8) A. Farrés, Á. Jorba, J.-M. Mondelo, and B. Villac. Periodic motion for an imperfect solar sail near an asteroid.

(9) H. Franz, L.A. D'Amario, L.L. Sackett, and et al. Wind lunar backflip and distant prograde orbit implementation. *Spaceflight Mechanics*, 108:999–1017, 2001.

(10) T. Noam, R. Karen, F. David, and T. Kimberly. Using solar radiation pressure to control l_2 orbits. *In the AAS/GFC International Symposium on Space Flight Dynamics*, 100(1):617–627, Greenbelt, Maryland, 11-15 May, 1998.

(11) R. L. Sohon. Attitude stabilisation by means of solar radiation pressure. *ARS Journal*, 29:371–373, 1995.

(12) S. Soldini, C. Colombo, and S. Walker. Comparison of hamiltonian structure-preserving and floquét mode station-keeping for libration-point orbits. *Proceedings of the AIAA/AAS Astrodynamics Specialist Conference*, AIAA-2014-4118, San Diego, California, 4-7 August 2014.

(13) D. J. Scheeres, F.-Y. Hsiao, and N X Vinh. Stabilizing motion relative to an unstable orbit: applications to spacecraft formation flight. *Journal of Guidance, Control and Dynamics*, 26(1):62–73, 2003.

(14) M. Xu and S. Xu. Structure-preserving stabilization for hamiltonian system and its applications in solar sail. *American Institute of Aeronautics and Astronautics*, 32(3):007–1004, 2009.

(15) R. W. Farquhar. Halo-orbit and lunar-swingby missions of the 1990's. *Acta Astronautica*, 24:227–234, 1991.

(16) L. Zaccarian and A. R. Teel. *Modern anti-windup synthesis: control augmentation for actuactors saturation*. Princeton university press, 2011.

(17) A. R. Teel. Global stabilization and restricted tracking for multiple integrators with bounded controls. *Sytems and Control Letters*, 18:165–171, 1992.

(18) V. Szebehely. *Theory of orbits in the restricted problem of three bodies*. Academic Press Inc., New York, 1967.

(19) W. S. Koon, M. W. Lo, J. E. Marsden, and S. D. Ross. *Dynamical systems, the three-body problem and space mission design*. Marsden Books, ISBN 978-0-615-24095-4, 2008.

(20) C. R. McInnes. Solar sailing: technology, dynamics and mission applications. *Springer*, Glasgow, Scotland, 1998.

(21) A. Farrés and Á. Jorba. A dynamical system approach for the station keeping of a solar sail. *The Journal of Astronautical Sciences*, 56(2):199–230, 2008.

(22) J. D. Biggs, C. McInnes, and T. Waters. New periodic orbits in the solar sail restricted three body problem. In *2nd Conference on Nonlinear Science and Complexity*.

(23) J.-M. Ginoux. Differential geometry applied to dynamical systems. *Nonlinear Science*, 66, 2009.

(24) G. Gómez, J. Llibre, R. Matínez, and C. Simó. Dynamics and mission design near libration points - volume i: Fundamentals: the case of collinear libration points, volume 2 of world scientific monograph series in mathematics. *World Scientific*, 2001.

(25) Y. Tsuda, O. Mori, R. Funase, H. Sawada, T. Yamamoto, T. Saiki, T. Endo, K. Yonekura, H. Hoshino, and J. Kawaguchi. Achievement of ikaros — japanese deep space solar sail demonstration mission. *Acta Astronautica*, 82(2):183–188, Elsevier, 2013.